Perovskite Solar Cells with Large-Area CVD-Graphene for Tandem Solar Cells

Felix Lang *, Marc A. Gluba, Steve Albrecht, Jörg Rappich, Lars Korte, Bernd Rech, and Norbert H. Nickel

Helmholtz-Zentrum Berlin für Materialien und Energie GmbH, Institut für Silizium Photovoltaik, Kekuléstr. 5, 12489 Berlin, Germany.

ABSTRACT: Perovskite solar cells with transparent contacts may be used to compensate thermalization losses of silicon solar cells in tandem devices. This offers a way to outreach stagnating efficiencies. However, perovskite top cells in tandem structures require contact layers with high electrical conductivity and optimal transparency. We address this challenge by implementing large area graphene grown by chemical vapor deposition as highly transparent electrode in perovskite solar cells leading to identical charge collection efficiencies. Electrical performance of solar cells with a graphene-based contact reached those of solar cells with standard gold contacts. The optical transmission by far exceeds that of reference devices and amounts to 64.3 % below the perovskite band gap. Finally, we demonstrate a four terminal tandem device combining a high band gap graphene-contacted perovskite top solar cell (E_g=1.6 eV) with an amorphous/crystalline silicon bottom solar cell (E_g=1.12 eV).

TOC GRAPHIC.

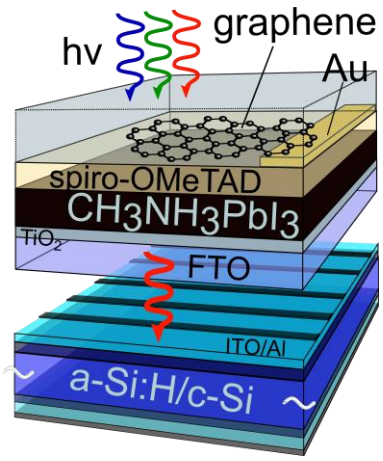

Hybrid perovskite methylammonium lead iodide ($CH_3NH_3PbI_3$) attracts ever-growing interest for use as a photovoltaic absorber.[1] Only recently, Jeon et al. demonstrated the great potential of this material in a single-junction solar cell with an efficiency of 18% [2].

Moreover, the low sub band gap absorption [3–6], increasing steeply to about $\alpha \approx 10^4$ cm^{-1} at 600 nm [7], enables semi-transparent perovskite solar cells to pre-filter the solar spectrum for low band gap absorbers in multi-junction devices. In particular, the combination with crystalline silicon (c-Si), which has a band gap of 1.12 eV at room temperature [8], is a promising route to circumvent thermalization losses in conventional photovoltaic energy conversion. By these means, conversion efficiencies beyond the Schockley-Queisser-limit are anticipated for perovskite/silicon tandem devices. [9,10]

Realizing a perovskite/silicon tandem design requires electrodes, which must be gently deposited onto organic layers of the hybrid perovskite top cell while being particularly transparent in the IR

spectral regime. Due to the unique optoelectronic properties of graphene this material is the clear choice to tackle this challenge. Electrodes based on graphene combine excellent optical transmission (T) of 97.4 % with a sheet resistance of 100 Ω/sq [11].

Apart from graphene, different strategies to contact the perovskite top cell have been proposed before, most of them suffering from a considerable amount of parasitic absorption at long wavelengths. Initial attempts based on 20 nm thin semi-transparent aluminium contacts achieve optical transmission of only 30 %. [12] Promising alternatives such as lamination of a silver nanowire (AgNW) mesh [10,13], poly(3,4-ethylenedioxythiophene) polystyrene sulfonate (PEDOT:PSS) layers [14], or carbon nanotube networks [15] have been proposed recently. Currently, the best performing perovskite/silicon tandem device with an energy conversion efficiency of 17.0 % [10] is based on AgNW electrodes. However, the maximum transmission of such electrodes is small compared to graphene and varies between 83 and 89.5 %, only.[16,17]

On the other hand, conventional transparent conductive oxides are optimized for spectral transmission but cannot be directly deposited onto the perovskite top cell. Ion bombardment during sputter deposition deteriorates the topmost hole-transport layer. Minimizing the damage of its organic material requires additional buffer layers and a meticulous control of the deposition process. [9] These buffer layers and their defective interfaces cause substantial current losses. [9]

While previous electrodes are limited either by electro-optical performance or processability, we demonstrate that graphene is a suitable contact material and is fully compatible to solution processing of perovskite solar cells. For this purpose, large-area graphene grown by chemical vapor deposition (CVD) [18,19] is transferred onto a perovskite solar cell consisting of the layer

sequence glass/SnO_2:F/TiO_2/$CH_3NH_3PbI_3$/spiro-OMeTAD. The latter abbreviates the hole conductor 2',7,7'-tetrakis-(N,N-di-4-methoxy-phenyl-amino)-9,9'-spirobifluorene. Figure 1 shows a sketch of the graphene based perovskite solar cell and the intended four terminal tandem device. It is important to note that the transfer process did not deteriorate the interface and bulk properties of the underlying hole conducting layer. Structural characterization of the used single layer graphene revealed the presence of wrinkles, nanoscale holes, and grain boundaries. However Raman backscattering revealed a negligible graphene D mode compared to the G and 2D resonances. In a recent report [20] on graphene contacts in perovskite solar cells an additional PEDOT:PSS layer was incorporated to enhance adhesion of graphene to the spiro-OMeTAD layer and to introduce field-effect doping in the graphene to lower the sheet resistance. Our data clearly shows that the PEDOT:PSS layer can be omitted, which renders the device structure less complex and results in a higher transparency. This is an important aspect for tandem solar cells. Details on the preparation of the solar cells can be found in the experimental section.

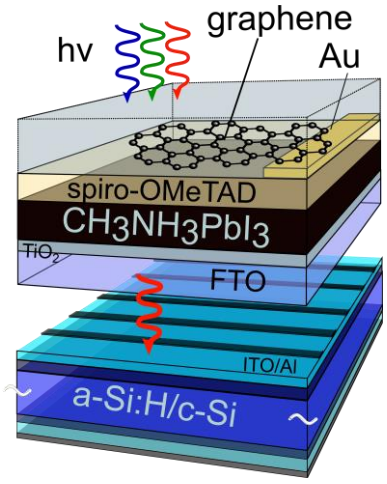

Figure 1. Simplified sketch of a four terminal tandem solar cell consisting of a graphene based perovskite top solar cell and an amorphous/crystalline silicon bottom solar cell. Figure not true to scale. The illumination direction of the perovskite top cell may be reversed.

In order to demonstrate the successful integration of graphene into the perovskite solar cell we compare the current-voltage (JV) characteristics of a perovskite solar cell with a graphene contact to a reference device containing a gold electrode (Fig. 2). Both solar cells were fabricated and analyzed side-by-side on the same substrate, to ensure comparability. The JV measurements are directly compared in reverse direction (from positive to negative bias). For clarity, the commonly observed hysteresis between forward and reverse measurements[21,22] is omitted in Fig. 2. The JV curves from forward and reverse measurements can be found in the supplementary information (Fig. S1). The electrical characteristics of the solar cells are summarized in Table 2.

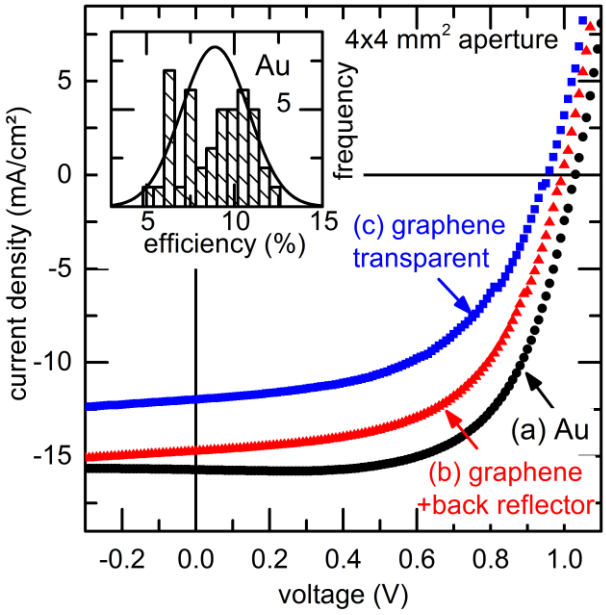

Figure 2. Current density-voltage characteristics of perovskite solar cells measured under AM1.5G conditions. (a) Reference solar cell with 80 nm Au contact. (b) Perovskite solar cell with graphene contact. The device was illuminated from the graphene side and a white diffusive reflector was used at the glass/SnO_2:F side. (c) Semi-transparent perovskite top cell with graphene contact illuminated from the glass/SnO_2:F side (without back reflector). The inset shows a histogram of measured solar cell efficiencies with Au contacts.

Cell Type	**η** (%)	**V_{OC}** (V)	**I_{SC}** (mA/cm^2)	**FF** (%)
(a) single, Au contact	10.2	1.03	15.75	62.9
(b) single, Graphene contact and back reflector	8.3	0.99	14.75	56.6
(c) top cell for tandem devices, Graphene contact	6.2	0.90	12.56	55.0

Table 1. Parameters of single perovskite solar cells (a, b) and top perovskite solar cell for use in tandem devices (c).

The black circles in Fig. 2 show the typical JV curve of a reference perovskite solar cell with standard Au contact. To check the reproducibility of the cell preparation, 42 cells were processed and the histogram of their efficiencies is plotted in the inset of Fig. 2. A mean value of $\eta = 8.9$ % is obtained with the highest efficiency amounting to $\eta = 12.4$ %. The power conversion efficiency of the reference cell prepared concurrently with the graphene/perovskite cell amounted to $\eta = 10.2$ %.

Since reflection at the gold contact effectively doubles the light path, we compare this reference solar cell to a graphene-contacted device with a Lambertian back reflector (red triangles in Fig. 2). The semi-transparent cell was illuminated from the graphene side with a

white paper used as reflector at the glass side. The open circuit voltage amounts to V_{OC} = 0.99 V, which is close to the V_{OC} of the Au reference solar cell (V_{OC} = 1.03 V). This clearly shows that a graphene contact can be successfully integrated in perovskite solar cells without deteriorating the device. Furthermore, the very similar V_{OC} shows that no substantial band offsets are introduced by the graphene contact. Remarkably, this was accomplished without the need for a buffer layer that promotes adhesion and field-effect doping. [20] Here, adhesion and intimate contact of graphene on spiro-OMeTAD is ensured by Van-der Waals forces.

The power conversion efficiency of the graphene/perovskite solar cell shows a somewhat lower value of η = 8.3 %. This is due to (i) a small contribution to the efficiency loss results from the short circuit current, J_{SC}, which decreases from 15.75 mA/cm^2 for the reference solar cell to 14.75 mA/cm^2 of the device with the graphene contact. This is not an issue of charge collection at the graphene electrode. In fact, the reduced J_{SC} is due to the lower photogeneration as result of the poor Lambertian back reflector. It has to be noted that also the entire device optic changed due to the switched illumination direction. Especially, parasitic absorption of the spiro-OMeTAD layer in the wavelength range from 300 to 450 nm becomes relevant since the device was illuminated from the graphene side. Moreover (ii) a reduction of the fill factor (FF) from 63 % on the Au reference to 57 % with graphene electrode contributes to the efficiency loss. A detailed analysis of the device parameters reveals an increase in series resistance from R_S = 10.7 Ωcm^2 in case of the Au electrode to 12.3 Ωcm^2 for the device with graphene electrode. R_S is estimated from the JV curves using $R_S = \left.\frac{dV}{dJ}\right|_{V=Voc}$. This increase in R_S is a direct consequence of the increase in electrode sheet resistance from ρ = 1.63 Ω/sq to ρ = 350 Ω/sq for Au and graphene contacts respectively.

The blue squares in Fig. 2 show the JV characteristics of the graphene/perovskite solar cell when illuminated from the glass/SnO_2:F side without a back reflector. This device geometry will be used later to demonstrate a perovskite/silicon tandem device. In this case, the light passes the solar cell only one time and therefore, the short circuit current decreases to J_{SC} = 12.56 mA/cm^2. Hence, the efficiency of the semi-transparent perovskite top cell amounts to $\eta = 6.2$ % when used in a four-terminal tandem device.

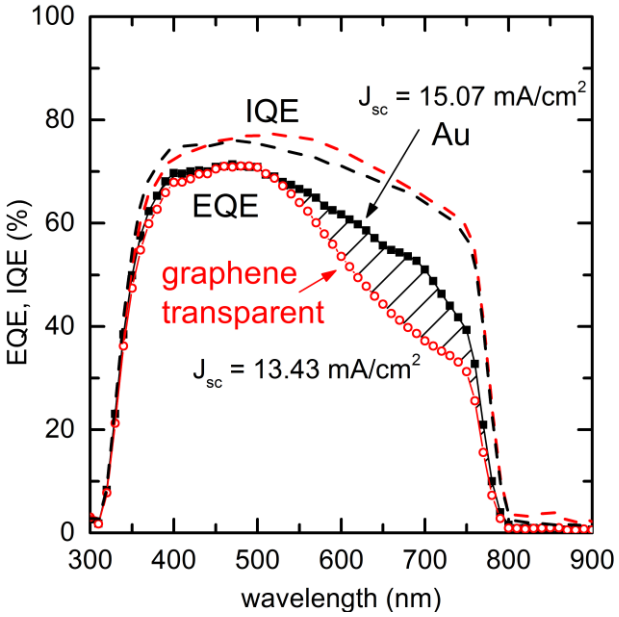

Figure 3. External (EQE) and internal quantum efficiency (IQE) spectra. The open red circles and full black squares correspond to the measured EQE of the graphene and Au contact, respectively. The red and black dashed lines correspond to the calculated IQE for graphene and Au contacts, respectively. The devices were illuminated from the glass/SnO_2:F side.

To substantiate the identical charge collection at the graphene contact with respect to the gold electrode the spectral response of both cells was measured. Figure 3 shows external (EQE) and internal (IQE) quantum efficiency measurements for the semi-transparent graphene/perovskite solar cell and the Au contacted reference cell. Both samples were illuminated from the

glass/SnO_2:F side. The EQE measured on the Au reference (solid squares in Fig. 3) reaches values of up to 71 % and an integrated current of 15.07 mA/cm^2. This integrated J_{SC} matches J_{SC} obtained from JV measurements (see Fig. 2). The EQE of the semi-transparent graphene/perovskite cell is reduced for wavelengths above 600 nm (open circles in Fig. 3). In this spectral regime the optical absorption in the perovskite starts to decrease and a considerable amount of light passes through the device without being absorbed. In a tandem device the transmitted light generates charge carriers in the bottom cell. Hence, changing the thickness of the perovskite absorber allows to adopt the transmittance of the top cell to the spectral response of the bottom cell.

The IQE is calculated from the reflection, $R(\lambda)$, and transmission, $T(\lambda)$, of the perovskite cell according to [23]

$$IQE(\lambda) = \frac{EQE(\lambda)}{1-R(\lambda)-T(\lambda)}. \quad (1)$$

The IQE of the graphene/perovskite solar cell (red dashed line in Fig. 2) reaches a maximum of 77.3 % at 520 nm. In comparison, the device with the Au contact shows a maximum of 76.1 %, only. Hence, graphene contacts show identical charge collection efficiency and light management even at long wavelengths.

In addition to the equal charge collection, the quantum efficiency of the semi-transparent graphene/perovskite solar cell suggests an optical benefit from using a graphene electrode. To elucidate the optical performance of this contact, the parasitic absorption within the graphene/perovskite device is analyzed in detail. For this purpose, diffuse transmission, reflection, and absorption of each individual layer are investigated.

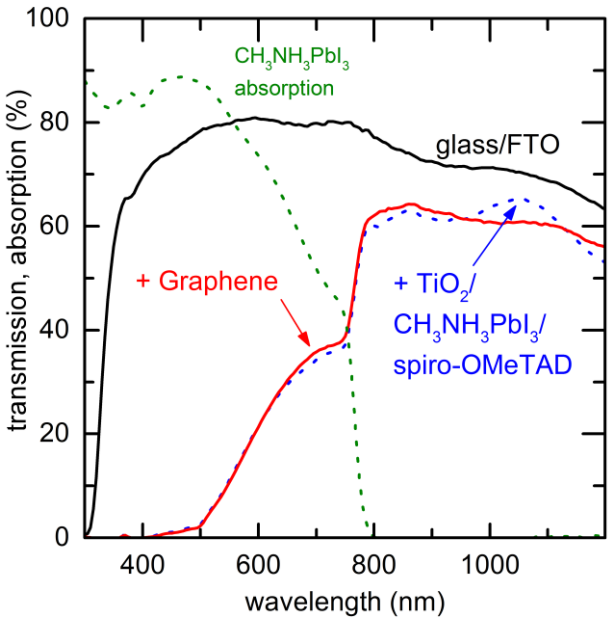

Figure 4. Transmission spectra of glass/SnO_2:F (solid black line), the perovskite top solar cell layer stack glass/SnO_2:F/TiO_2/$CH_3NH_3PbI_3$/spiro-OMeTAD (dotted blue line), and of glass/SnO_2:F/TiO_2/$CH_3NH_3PbI_3$/spiro-OMeTAD/graphene/support (solid red line). Absorption of $CH_3NH_3PbI_3$ on glass (dotted olive line).

Figure 4 shows the optical absorption of the $CH_3NH_3PbI_3$ perovskite absorber on glass (olive dashed line) and the transmission of the glass/SnO_2:F substrate (solid black line). The perovskite absorber shows a broad absorption tail from over 80 % absorption at a wavelength of $\lambda \approx 500$ nm to around 40 % at $\lambda \approx 750$ nm. The SnO_2:F reaches a maximum transmission of 80 % at around 600 nm. At longer wavelengths the transmission decreases to about 65 % due to free carrier absorption.[24]

Although the absorption of the perovskite is low in the sub band gap region, the transmission of the device prior to the graphene transfer (dotted blue line in Fig. 4) is reduced to 60 %, only. This is due to enhanced reflection at the spiro-OMeTAD/air interface.

To evaluate the optical impact of the graphene contact a direct comparison between the transmission of the perovskite solar cell stack with and without graphene is of particular interest. The red solid line in Fig. 4 shows the transmission of the complete device structure including graphene and its polymer-support. Remarkably, an increase of the absolute transmission of around 2 %, compared to the sample without graphene/support is observed for $650 < \lambda < 950$ nm. This effect is due to a reduced reflection at the spiro-OMeTAD/graphene/support versus the spiro-OMeTAD/air interface. A decrease in transmission observed for $950 < \lambda < 1130$ nm is due to increased reflection, caused by the same interference effect. This anti-reflection effect of the graphene contact including its polymer support enhances the optical transmission of the semi-transparent perovskite solar cell. These beneficial effects even predominate the absorption at the graphene contact itself, since the optical absorption of monolayer graphene amounts to 2.3 %, only.

The complete graphene/perovskite solar cell transmits 64.3 % of the incident light at 860 nm. The transmitted light can be harvested in the bottom part of a tandem device. For this purpose, the semi-transparent graphene/perovskite top cell is integrated into a four terminal tandem design. This arrangement is particularly favourable, since it does not require current matching. As an example we present the combination with an amorphous/crystalline silicon (a-Si:H/c-Si) [25] heterojunction solar cell as the bottom device. Other low band gap solar cells, e.g. organic or chalcopyrite-based, may also be used for the bottom device.

Figure 5 shows the measured EQE, IQE and JV curves of the a-Si:H/c-Si solar cell measured as single device (open circles) and as bottom solar cell with a graphene based perovskite top solar cell as optical filter (full squares).

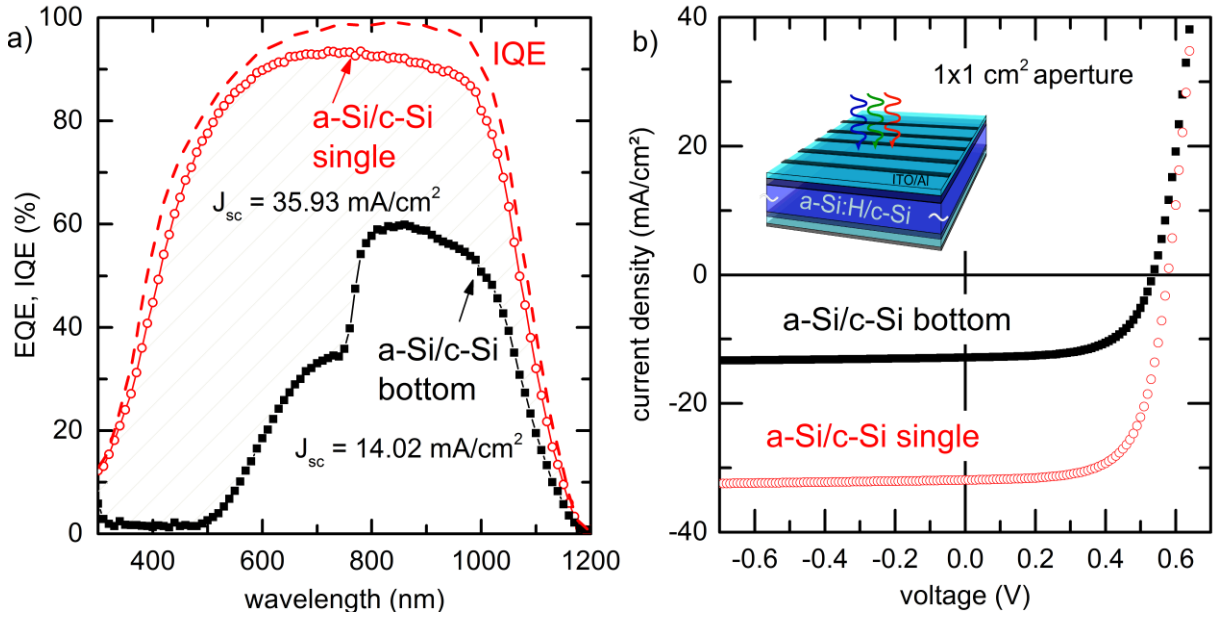

Figure 5. a) External and internal quantum efficiency spectra of the single a-Si:H/c-Si solar cell, (open circles EQE, dashed line IQE), and EQE of the a-Si:H/c-Si bottom solar cell, measured with graphene based perovskite solar cell as optical filter (full squares). b) Current density-voltage characteristics of the single a-Si:H/c-Si solar cell, (open red circles), and the a-Si:H/c-Si bottom solar cell under reduced light intensity calibrated to match J_{SC} as obtained from the EQE measurement.

The single a-Si:H/c-Si solar cell shows a typical EQE and IQE with maxima of 93 % and 98 %, respectively. The integrated current amounts to 35.93 mA/cm^2 for this unoptimized device. Assuming an ideal high band gap top solar cell, the EQE of an a-Si:H/c-Si solar cell as bottom device is expected to vanish for $\lambda < 775$ nm, while being unaffected for $\lambda > 775$ nm. Using the graphene/perovskite solar cell as optical filter, the a-Si:H/c-Si solar cell EQE reduces to 60 % at 860 nm (full squares, Fig. 5). This correlates with the transmission of the graphene/perovskite solar cell with a maximum of 64.3 % at 860 nm. For $\lambda < 800$ nm the EQE follows the perovskite

solar cell transmission spectrum as plotted in Fig. 4. The integrated current of the a-Si:H/c-Si bottom cell is reduced by a factor of 2.5 to 14 mA/cm^2 compared to a single a-Si:H/c-Si heterojunction. The reduced light intensity further influences V_{OC} of the a-Si:H/c-Si solar cell in a logarithmic way as expected from diode characteristics. [26] Table 2 summarizes photovoltaic parameters of a-Si:H/c-Si solar cells as single (a) and bottom (b) solar cells. Due to the decrease in J_{SC} and V_{OC} the efficiency reduces from 18.5 % to 7.0 % with a graphene/perovskite solar cell as optical filter.

Cell type	η (%)	V_{oc} (V)	J_{sc} (mA/cm^2)	FF (%)
(a) a-Si:H/c-Si single	18.5	0.71	36.1	72.1
(b) a-Si:H/c-Si bottom	7.0	0.67	14.0	73.8
(c) perovskite top	6.2	0.90	12.6	55.0
(d) projected tandem	13.2			

Table 2. Summarized solar cell parameters: (a) the a-Si:H/c-Si single solar cell, (b) the a-Si:H/c-Si solar cell as bottom solar cell in a 4-terminal tandem with a graphene based perovskite top cell as optical filter, (c) the graphene based perovskite top solar cell, and (d) the perovskite/a-Si:H/c-Si four terminal tandem efficiency .

As a proof of concept, the semi-transparent perovskite solar cell and the a-Si:H/c-Si solar cell are assembled into a tandem device. The efficiency of such a four terminal tandem solar cell amounts to 13.2 %. This is a relative increase of 30 % compared with the single perovskite solar cell with typical Au contacts (see Tab. 1 and Tab. 2). The efficiency of the presented tandem solar cell is comparable to recent results obtained with four terminal tandem designs using ITO electrodes [9]. It is important to note, that no anti-reflection (AR) coating was used for the perovskite top solar cell.

In summary, electrodes based on large area CVD-graphene combine a flexible transfer process and unique optoelectronic properties. They therefore provide an excellent approach for the realisation of perovskite/silicon tandem solar cells surpassing the Schockley-Queisser-limit for single junction solar cells. We showed the successful implementation of a transparent large area, high quality single layer graphene contact in perovskite solar cells. Electrical performance of solar cells based on the layer sequence glass/SnO_2:F/TiO_2/$CH_3NH_3PbI_3$/spiro-OMeTAD/graphene reached those of perovskite solar cells with standard Au contact. In detail, identical open circuit voltages of around 1 V as well as identical charge collection efficiencies proved defect free implementation of the monolayer graphene contact. Therefore, the presented spiro-OMeTAD/graphene electrode can be used in four terminal and monolithic perovskite tandem solar cells. A high series resistance can be reduced with the use of multiple graphene layers.[11,20] Graphene/perovskite solar cells showed a high optical transmission below the perovskite band gap (64.3 % at 860 nm). These semi-transparent perovskite solar cells (η = 6.20 %) were integrated in a four terminal tandem device with an a-Si:H/c-Si bottom solar cell (η = 7.0 %). Power conversion efficiency of the tandem device was 13.2 %, thus increased by 30% as compared to the respective perovskite single junction cell.

EXPERIMENTAL METHODS

Perovskite Solar Cell Preparation

Planar perovskite solar cells were prepared following the well-established layer sequence glass/FTO/TiO_2/$CH_3NH_3PbI_3$/spiro-OMeTAD. Therefore a ca. 40 nm thick compact TiO_2 layer was prepared by spray pyrolysis from titanium diisopropoxide bis(acetylacetonate) ($Ti(acac)_2OiPr_2$, Sigma Aldrich) at 460 ºC on glass/SnO_2:F substrates (R = 8 Ω/sq, Solaronix). Prior to the deposition the substrates were cleaned with detergent/H_2O, acetone and isopropanol. After deposition they were fired at 450 ºC for 30 min. A stoichiometric $CH_3NH_3PbI_3$ precursor solution containing 0.8 M of PbI_2 (Sigma Aldrich) and CH_3NH_3I (synthesized from CH_3NH_2 and HI [6], Sigma Aldrich) in the mixed solvent γ-butyrolactone (GBL) and dimethyl sulfoxide (DMSO) with volume ratio 70/30 (v.%/v.%) was prepared under stirring at 60°C for 12 h. A 300 nm thick $CH_3NH_3PbI_3$ layer was spin coated at 1000 rpm for 10 s and 2000 rpm for 20 s. In the final spin coating stage 150 µl toluene were dripped onto the sample, according to Ref. [27]. The obtained $CH_3NH_3PbI_3$ layer was dried on a hotplate at 100 ºC for 10 min. After cooling to room temperature the hole conductor 2,2',7,7'-tetrakis-(N,N-di-4-methoxy-phenyl-amino)-9,9'-spirobifluorene (spiro-OMeTAD, Merck) is applied by spin coating at 2000 rpm for 30 s, and left for 12 h in N_2 atmosphere. The spin coating formulation contained 80 mg spiro-OMeTAD dissolved in 1 ml chlorobenzene, 46.4 µl of a bis(trifluoromethane) sulfonimide lithium salt (LiTFSI, Lumtec) stock solution (170 mg/ml in acetonitrile), and 8.5 µl of 4-tert-butylpyridine (Sigma Aldrich). Finally, gold electrodes were deposited by thermal evaporation at a base pressure of 10^{-7} mbar with a rate of 0.7 Å/s. The active area of perovskite solar cells was defined using a 0.16 cm^2 shadow mask. Since the perovskite film formation is sensitive to humidity all preparation steps were performed under N_2 atmosphere. An anti-reflection coating was omitted.

Graphene Electrode Preparation

Large area CVD-graphene sheets were prepared via catalytic decomposition of methane on a hot 25 µm thick copper foil [18,19]. Prior to the graphene deposition, the copper substrate was polished and sonicated in acetone and isopropyl alcohol for 10 min. Residual surface oxides were removed using acetic acid. The chemical vapour deposition of graphene is conducted in a two-step process: First, the copper substrate is recrystallized in a hydrogen flow of 2 sccm at a temperature of 1000°C. Subsequently, the hydrogen flow was reduced to 0.7 sccm and 11.4 sccm of the carbon precursor methane was introduced. The latter growth step was carried out at a pressure of 0.5 mbar for one hour. The final graphene sheets had a typical size of several square centimeters. From these sheets smaller pieces of about 1 cm^2 were cut and used as transparent electrodes. The graphene electrode was contacted using a Au grid finger, which was evaporated onto spiro-OMeTAD. For optical and electrical characterization graphene sheets were transferred onto a 300 nm SiO_2 layer on a c-Si wafer. According to Hall-effect measurements performed in the van-der-Pauw geometry the graphene sheets are p-type showing a hole mobility of 1020 cm^2/Vs and a sheet resistance of 350 Ω/sq.

a-Si:H/c-Si Solar Cell Preparation & Characterisation

Silicon heterojunction solar cells based on an n-type mono-crystalline silicon (c-Si) wafer and thin hydrogenated amorphous silicon (a-Si:H) layers are used as bottom solar cell in a 4-terminal tandem solar cell structure. The a-Si:H/c-Si solar cell preparation was performed according to Ref. [25]. Intrinsic a-Si:H layers are used for passivation of the c-Si surface enabling open-circuit voltages larger than 700 mV. The a-Si:H/c-Si solar cell had a V_{OC} of 709 mV and an J_{SC} of 35.93 mA/cm^2.

IV, EQE and UV-vis characterisation

Current-voltage measurements of perovskite solar cells were performed using a "Steuernagel Lichtechnik" sun simulator, mimicking AM 1.5G spectra. Solar cells with graphene and Au reference electrodes were prepared and measured side by side on the same substrate. Cell size of the a-Si:H/c-Si solar cell was 1 cm^2, while perovskite cell size was 0.16 cm^2 in case of the Au reference electrode. CVD-graphene based electrodes had an area of 1.03 cm^2, including the Au finger grid while being measured with an aperture of 0.16 cm^2 in size. All JV measurements were performed in forward (from neg. to pos.) and reverse direction. A delay time of 40 ms with 20 ms acquisition time, corresponding to a scan speed of 0.167 V/s was chosen. According to Refs [21,22] such a scan speed causes a clear appearance of the hysteresis effect, while slower and faster measurements result in a smaller hysteresis of the JV curves. External quantum efficiencies were measured on identically prepared samples without bias illumination. EQE of the perovskite top solar cell was measured with a black absorber behind it. On the other hand EQE of the bottom cell was measured with the perovskite solar cell as optical filter. IQE was determined from reflection (R) and transmission (T) according to $\mathrm{IQE}(\lambda) = \frac{\mathrm{EQE}(\lambda)}{1-\mathrm{R}(\lambda)-\mathrm{T}(\lambda)}$. Diffuse transmission and reflection was measured with a Perkin Elmer UV-vis spectrometer, equipped with an integrating Ulbricht sphere and calibrated from an ISE certified white standard.

AUTHOR INFORMATION

Corresponding Author

Felix Lang, e-mail felix.lang@helmholtz-berlin.de, Phone: +00 49 30 8062 41354, Fax +49 30 8062-41333

Author Contributions

The manuscript was written through contributions of all authors. All authors have given approval to the final version of the manuscript.

Funding Sources

The authors are grateful to the 'Helmholtz-Alliance and the Initiative and Networking Fund of the Helmholtz Association' for funding.

ACKNOWLEDGMENT

The authors thank Rodrigo Sáez Araoz from the institute for heterogeneous material systems, for support in TiO_2 spray pyrolysis. Tobias Hänel and Karolina Mack from the Competence Centre Thin-Film- and Nanotechnology for Photovoltaics Berlin (PVcomB) are acknowledged for support in EQE and UV-vis measurements. The a-Si:H/c-Si solar cells were provided by J. Kegel, E. Conrad, and M. Mews.

Supporting Information Available: Current density-voltage characteristics of perovskite solar cells in forward and reverse direction for Au and graphene electrodes respectively. This material is available free of charge via the Internet. http://pubs.acs.org

ABBREVIATIONS

silver nanowire, AgNW; poly(3,4-ethylenedioxythiophene) polystyrene sulfonate , PEDOT:PSS; carbon nanotube networks, CNT; chlorobenzene, CBZ; γ-butyrolactone, GBL; dimethyl sulfoxide, DMSO; crystalline silicon, c-Si; anti-reflection, AR; titanium diisopropoxide bis(acetylacetonate), $Ti(acac)_2OiPr_2$; open circuit voltage, $V_{OC;}$ fill factor, FF; short circuit current, Jsc; current-voltage, IV; transmission, T; transparent conductive oxide, TCO; indium tin

oxide, ITO; fluorine doped tin oxide, SnO_2:F; hole transport material, HTM; external quantum efficiency, EQE; internal quantum efficiency, IQE; chemical vapour deposition, CVD; 2,2',7,7'-Tetrakis-(N,N-di-4-methoxy-phenyl-amino)-9,9'-spirobifluorene, spiro-OMeTAD

REFERENCES

(1) Hodes, G. Perovskite-Based Solar Cells. *Science* **2013**, *342*, 317–318.

(2) Jeon, N. J.; Noh, J. H.; Yang, W. S.; Kim, Y. C.; Ryu, S.; Seo, J.; Seok, S. Il. Compositional Engineering of Perovskite Materials for High-Performance Solar Cells. *Nature* **2015**, *517*, 476–480.

(3) Umari, P.; Mosconi, E.; De Angelis, F. Relativistic GW Calculations on $CH_3NH_3PbI_3$ and $CH_3NH_3SnI_3$ Perovskites for Solar Cell Applications. *Sci. Rep.* **2014**, *4*, 4467.

(4) Löper, P.; Stuckelberger, M.; Niesen, B.; Werner, J.; Filipič, M.; Moon, S.-J.; Yum, J.-H.; Topič, M.; De Wolf, S.; Ballif, C. Complex Refractive Index Spectra of $CH_3NH_3PbI_3$ Perovskite Thin Films Determined by Spectroscopic Ellipsometry and Spectrophotometry. *J. Phys. Chem. Lett.* **2015**, *6*, 66–71.

(5) Yin, W. J.; Shi, T.; Yan, Y. Unique Properties of Halide Perovskites as Possible Origins of the Superior Solar Cell Performance. *Adv. Mater.* **2014**, *26*, 4653–4658.

(6) Baikie, T.; Fang, Y.; Kadro, J. M.; Schreyer, M.; Wei, F.; Mhaisalkar, S. G.; Graetzel, M.; White, T. J. Synthesis and Crystal Chemistry of the Hybrid Perovskite $(CH_3NH_3)PbI_3$ for Solid-State Sensitised Solar Cell Applications. *J. Mater. Chem. A* **2013**, *1*, 5628–5641.

(7) Xing, G.; Mathews, N.; Lim, S. S.; Yantara, N.; Liu, X.; Sabba, D.; Grätzel, M.; Mhaisalkar, S.; Sum, T. C. Low-Temperature Solution-Processed Wavelength-Tunable Perovskites for Lasing. *Nat. Mater.* **2014**, *13*, 476–480.

(8) Thurmond, C. D. The Standard Thermodynamic Functions for the Formation of Electrons and Holes in Ge, Si, GaAs, and GaP. *J. Electrochem. Soc.* **1975**, *122*, 1133–1141.

(9) Löper, P.; Moon, S.-J.; Martin de Nicolas, S.; Niesen, B.; Ledinsky, M.; Nicolay, S.; Bailat, J.; Yum, J.-H.; De Wolf, S.; Ballif, C. Organic-Inorganic Perovskite/crystalline Silicon Four-Terminal Tandem Solar Cells. *Phys. Chem. Chem. Phys.* **2014**, 1619–1629.

(10) Bailie, C. D.; Christoforo, M. G.; Mailoa, J. P.; Bowring, A. R.; Unger, E. L.; Nguyen, W. H.; Burschka, J.; Pellet, N.; Lee, J. Z.; Grätzel, M.; *et al.* Semi-Transparent Perovskite Solar Cells for Tandems with Silicon and CIGS. *Energy Environ. Sci.* **2014**, *8*, 956–963.

(11) Bae, S.; Kim, H.; Lee, Y.; Xu, X.; Park, J.-S.; Zheng, Y.; Balakrishnan, J.; Lei, T.; Kim, H. R.; Song, Y. Il; *et al.* Roll-to-Roll Production of 30-Inch Graphene Films for Transparent Electrodes. *Nat. Nanotechnol.* **2010**, *5*, 574–578.

(12) Todorov, T.; Gershon, T.; Gunawan, O.; Sturdevant, C.; Guha, S. Perovskite-Kesterite Monolithic Tandem Solar Cells with High Open-Circuit Voltage. *Appl. Phys. Lett.* **2014**, *105*, 173902–173906.

(13) Guo, F.; Azimi, H.; Hou, Y.; Przybilla, T.; Hu, M.; Bronnbauer, C.; Langner, S.; Spiecker, E.; Forberich, K.; Brabec, C. J. High-Performance Semitransparent Perovskite Solar Cells with Solution-Processed Silver Nanowires Top Electrodes. *Nanoscale* **2014**, *7*, 1642–1649.

(14) Jiang, F.; Liu, T.; Zeng, S.; Zhao, Q.; Min, X.; Li, Z. Metal Electrode – Free Perovskite Solar Cells with Transfer-Laminated Conducting Polymer Electrode. **2015**, *23*, 3748–3754.

(15) Li, Z.; Kulkarni, S. a; Boix, P. P.; Shi, E.; Cao, A.; Fu, K.; Batabyal, S. K.; Zhang, J.; Xiong, Q.; Wong, L. H.; *et al.* Laminated Carbon Nanotube Networks for Metal Electrode-Free Efficient Perovskite Solar Cells. *ACS Nano* **2014**, *8*, 6797–6804.

(16) Mailoa, J. P.; Bailie, C. D.; Johlin, E. C.; Hoke, E. T.; Akey, A. J.; Nguyen, W. H.; McGehee, M. D.; Buonassisi, T. A 2-Terminal Perovskite/silicon Multijunction Solar Cell Enabled by a Silicon Tunnel Junction. *Appl. Phys. Lett.* **2015**, *106*, 121105.

(17) Guo, F.; Zhu, X.; Forberich, K.; Krantz, J.; Stubhan, T.; Salinas, M.; Halik, M.; Spallek, S.; Butz, B.; Spiecker, E.; *et al.* ITO-Free and Fully Solution-Processed Semitransparent Organic Solar Cells with High Fill Factors. *Adv. Energy Mater.* **2013**, *3*, 1062–1067.

(18) Gluba, M. A.; Amkreutz, D.; Troppenz, G. V.; Rappich, J.; Nickel, N. H. Embedded Graphene for Large-Area Silicon-Based Devices. *Appl. Phys. Lett.* **2013**, *103*, 073102–073105.

(19) Li, X.; Cai, W.; An, J.; Kim, S.; Nah, J.; Yang, D.; Piner, R.; Velamakanni, A.; Jung, I.; Tutuc, E.; *et al.* Large-Area Synthesis of High-Quality and Uniform Graphene Films on Copper Foils. *Science* **2009**, *324*, 1312–1314.

(20) You, P.; Liu, Z.; Tai, Q.; Liu, S.; Yan, F. Efficient Semitransparent Perovskite Solar Cells with Graphene Electrodes. *Adv. Mater.* **2015**, *27*, 3632–3638.

(21) Unger, E. L.; Hoke, E. T.; Bailie, C. D.; Nguyen, W. H.; Bowring, A. R.; Heumuller, T.; Christoforo, M. G.; McGehee, M. D. Hysteresis and Transient Behavior in Current-Voltage Measurements of Hybrid-Perovskite Absorber Solar Cells. *Energy Environ. Sci.* **2014**, *7*, 3690–3698.

(22) Snaith, H. J.; Abate, A.; Ball, J. M.; Eperon, G. E.; Leijtens, T.; Noel, N. K.; Stranks, S. D.; Wang, J. T.-W.; Wojciechowski, K.; Zhang, W. Anomalous Hysteresis in Perovskite Solar Cells. *J. Phys. Chem. Lett.* **2014**, 1511–1515.

(23) Dittrich, T. *Materials Concepts for Solar Cells*; 1st ed.; Imperial College Press: London, 2014.

(24) Yu, P.; Cardona, M. *Fundamentals of Semiconductors: Physics and Materials Properties*; 3rd ed.; Springer-Verlag: Berlin, 2005.

(25) Kegel, J.; Angermann, H.; Stürzebecher, U.; Conrad, E.; Mews, M.; Korte, L.; Stegemann, B. Over 20% Conversion Efficiency on Silicon Heterojunction Solar Cells by IPA-Free Substrate Texturization. *Appl. Surf. Sci.* **2014**, *301*, 56–62.

(26) Sze, S. M. *Physics of Semiconductor Devices*; 2nd ed.; John Wiley & Sons, Inc: New York, 1981.

(27) Jeon, N. J.; Noh, J. H.; Kim, Y. C.; Yang, W. S.; Ryu, S.; Seok, S. Il. Solvent Engineering for High-Performance Inorganic-Organic Hybrid Perovskite Solar Cells. *Nat. Mater.* **2014**, *13*, 897–903.